Journal of Applied Mathematics and Physics, 2025, 13(8), 2674-2691
https://www.scirp.org/journal/jamp
ISSN Online: 2327-4379
ISSN Print: 2327-4352

Analysis and Estimation of the Vertical Drift Velocity from the Ionization Production Velocity in Correspondence with Radar Data from Jicamarca and IRI 2020

Abdoul Kader Segda[1,2*], Salfo Kaboré[1,2], Aristide Gybre[1,2], Madougou Saidou[3], Frédéric Ouattara[1,2]

[1]Laboratory of Analytical Chemistry, Space Physics and Energy (LACAPSE), Koudougou, Burkina Faso
[2]Department of Physics, Norbert ZONGO University (UNZ), Koudougou, Burkina Faso
[3]Department of Physics, Ecole Normale Supérieure, University Abdou Moumouni, Niamey, Niger
Email: *ksegda1@gmail.com

How to cite this paper: Segda, A.K., Kaboré, S., Gybre, A., Saidou, M. and Ouattara, F. (2025) Analysis and Estimation of the Vertical Drift Velocity from the Ionization Production Velocity in Correspondence with Radar Data from Jicamarca and IRI 2020. *Journal of Applied Mathematics and Physics*, **13**, 2674-2691.
https://doi.org/10.4236/jamp.2025.138152

Received: June 24, 2025
Accepted: August 19, 2025
Published: August 22, 2025

Abstract

This study presents an analytical model for estimating the ionospheric vertical drift velocity. This model is based on the time derivative of a proposed formula for solar radiation power, which yields an "ionization production velocity". A key model parameter, the "production factor" (k), is calibrated against published radar data from Jicamarca and IRI-2020 model outputs to generate diurnal drift profiles for specific equatorial locations. Thus, referring to the evening peak of the radar data from Jicamarca, the model by the production speed shows that 1) for the same latitude, the higher the production factor, the greater the drift or production speed and 2) for two geographical positions of different latitudes and: a) For the same drift or production speed, the further one moves away from the equator, the more the production factor decreases. b) For the same production factor, the further one moves away from the equator, the greater the production or drift speed. With IRI 2020 we arrive at the same conclusions across the two cities of Conakry and Sikasso. Sikasso, being further from the equator than Conakry presents a smaller production factor 236.19 against 240.69 with a drift speed of 31.89 $m{\cdot}s^{-1}$ for the 6 H peak and 27.11 $m{\cdot}s^{-1}$ for the 14 H peak while Conakry presents respectively 30.02 $m{\cdot}s^{-1}$ and 25.52 $m{\cdot}s^{-1}$. As for the average speed, Conakry presents an average speed from 0 H to 24 H of 15.90 $m{\cdot}s^{-1}$ while Sikasso is 16.99 $m{\cdot}s^{-1}$. IRI 2020 offers almost the same peak drift speeds but at noon with however discrepancies for the morning peaks. However, there are other estimation methods. Finally, the production method is important because it allows for different modeling.

Keywords

Speed, Drift, Production, Jicamarca, IRI

1. Introduction

The ionosphere is the ionizable part of the atmosphere extending from 60 km to more than 650 km. During the day, depending on the electron density, the ionosphere will be subdivided into four sub-layers: the D, E, F1 and F2 sub-layers. At night, of the four sub-layers observed during the day, only the E and F2 sub-layers will remain, which will be characterized on the one hand by low electron densities and on the other hand by observation altitudes of these ionization maxima even higher than those observed during the day. The ionosphere, thus described succinctly, still presents differential characteristics depending on the latitudes. For example, 1) the northern and southern lights are characteristic of the polar regions or those close to the poles, also called high latitudes. During its auroras, the ionosphere in these parts lights up in different colors due to the interactions of particles from the sun called solar wind with the plasma of the ionosphere. These particles, due to the protective magnetosphere, end up penetrating into the upper ionosphere of the poles through the North and South polar horns, which result from the opening in these parts of the Earth's magnetic field lines. Also, 2) at low latitudes centered on the geographic equator the ionosphere is characterized by a particular daytime structure called Equatorial Ionization Anomaly (EIA) [1] or Appleton anomaly [2]. Indeed, during the day and at latitudes from 20˚N to 20˚S we will observe a gutter structure in the NmF2 ionization density maxima and a dome structure of the observation altitudes of these HmF2 ionization maxima centered on the equator. The plausible explanation for many authors to justify this Anomaly would be due to the upward vertical drift called Hall drift [3] of the ionized plasma from the lower layers of the equator to the upper layers or subsequently this ionized plasma will diffuse through the Earth's magnetic field lines to descend deeper and deeper from the equator to the latitudes of the maximum density peaks. The transport mechanism responsible for this Equatorial Ionization Anomaly is the velocity $\boldsymbol{V}$ which results from the vector product of the Earth's magnetic field $\boldsymbol{B}$ which is horizontal to the equator and oriented towards the North with the electric field $\boldsymbol{E}$ generated by the ionospheric currents which will be called equatorial electrojet (EEJ) [4] circulating towards the East in the sub-layer E. Also the fluctuations of the component of the Earth's magnetic field will often cause an inversion of the ionospheric current which will be called Counter-electrojet (CEJ) [5] which will be predominant in the afternoons and observable by a peak in the critical frequencies foF2. Thus an explanation for the profile B in the diurnal variability of the critical frequencies foF2 which presents an ionization peak in the morning and in the afternoon separated by a trough around noon is found. The morning peak is due to an electrojet (EJ) that of the evening to a coun-

ter-electrojet (CEJ) and the trough to the vertical drift.

Thus the equatorial ionosphere will be investigated by many measuring instruments both on the ground [6] and in the air [7] (coherent and incoherent scattering radars, ionosondes and magnetometers) in order to have good estimates on the vertical drift speed of the ionized plasma. The very first precursor radar deployed for this purpose was the incoherent scattering radar of Jicamarca in 1968 [8], which measured the vertical drift speeds of the plasma of the F sub-layer of the equatorial ionosphere between 200 and 800 km with a temporal resolution of 1 to 5 mn and latitudinal resolution of 15 to 25 km. From these data, several studies or works have been the subject of publications such as those of [9]. Later, other models [10] using data from the JULIA radar which experimented with a measurement system using the Doppler effect or others such as COSMIC or ROCSAT-1 (Taiwan Region's Satellite) were used for measurements of the vertical drift speed. Thus, in the same dynamic of contributing to a better understanding of the vertical drift, we propose in this article to provide another approach to estimating the vertical drift which is that of the ionization production speed. Indeed, if the vertical drift testifies to a lack or departure of ionization, it would testify in parallel to this effect in another vision of a production whose quantity would be inversely proportional to that of the derived ionized plasma. By this approach, accompanied by formula we could, in reference to radar data from Jicamarca or others like IRI 2020 found both in times of calm and magnetic disturbance, the ionization profiles at all latitudes and longitude sectors. To do this, the article will be structured essentially in three parts which are the methodology, the results and the discussion part.

2. Methodology

The methodology consisted of presenting the ionized part of the ionosphere as a rigid block capable of reflecting waves by its densification surface which will be located by a position vector. The displacement $h(t)$ of this densification surface will be proportional to the variation in the power of solar radiation $P_0(t)$ [11] which is the main ionization factor.

$$\begin{cases} h(t) = k\dfrac{\mathrm{d}P_0(t)}{\mathrm{d}t} \\ P_0(t) = 2\sin\left(\dfrac{\pi}{12}t\right)\cos\left(\dfrac{\pi}{6}t\right) \end{cases} \tag{1}$$

A downward movement will indicate that the solar radiation is increasing in power or pressing and an upward movement will indicate the opposite. Thus, knowing the expression of the position vector, its derivative will allow us to obtain the speed vector which we will call the production vector $V_P(t)$ because as shown in **Figure 1** below its minus sign (−) indicates an increasingly pronounced production and the (+) sign indicates a less and less pronounced production.

By adjusting the production factor, we find the same evening peak speed with the Jicamarca radar data and thus obtain the corresponding ionization or drift

profile. With the IRI 2020 data and from the cities of Conakry and Sikasso dedicated to the study, we first find the average speed of the day. From this average speed we go back to find the ionization factor. From the ionization factor we find the drift and production profiles. From these profiles we identify the drift speed peaks in each range.

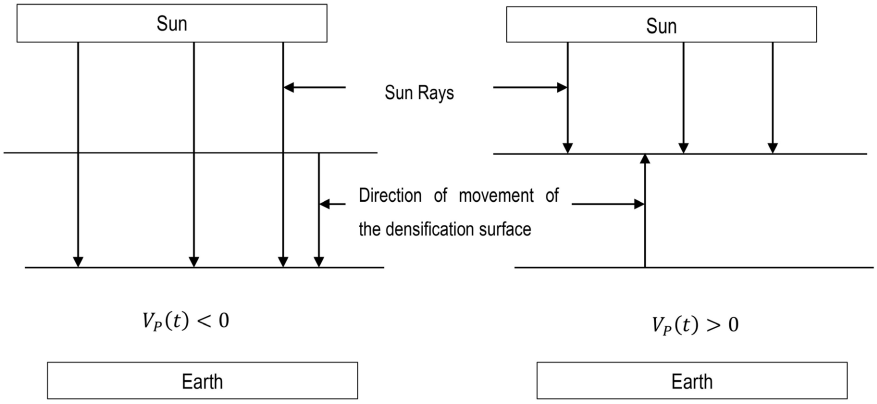

Figure 1. Displacement of the densification surface by solar rays.

Thus described the coefficient of proportionality k will be called production factor and will be expressed in meters per Watt (m/W). Also because k is also a constant then the displacement of the ionization densification surface $h(t)$ will be the time derivative of a power of solar radiation of the form k. $P_0(t)$ or $2k$ would be the amplitude. $h(t)$ Obtained is of the form:

$$h(t)=\frac{\pi}{6}k\left[\cos\left(\frac{\pi}{4}t\right)-\sin\left(\frac{\pi}{12}t\right)\sin\left(\frac{\pi}{6}t\right)\right] \tag{2}$$

The temporal variation of the power of solar radiation and therefore of the displacement of the densification surface will present the following profile **Figure 2**.

If we consider the spherical reference frame as shown in **Figure 3** below as an example or the position of a point M is identified by (r,θ,φ) called spherical coordinates in reference to the direct orthonormal spherical basis $(\boldsymbol{e}_r,\boldsymbol{e}_\theta,\boldsymbol{e}_\varphi)$.

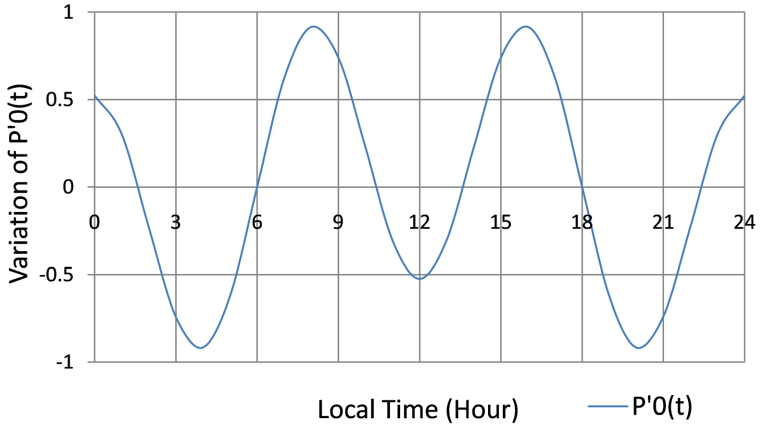

Figure 2. Variability profile of the displacement of the densification surface.

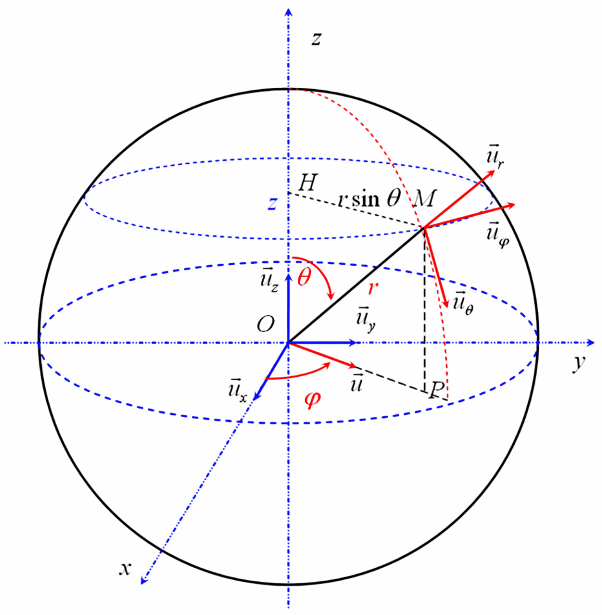

Figure 3. Coordinate systems.

The position vector $\boldsymbol{OM}$ and that of the speed vector $\boldsymbol{V}_{M/R_0}$ will be noted in this reference framework $R_0\left(O,\boldsymbol{e}_r,\boldsymbol{e}_\theta,\boldsymbol{e}_\varphi\right)$ by the following expressions:

$$\begin{cases}\boldsymbol{OM}=r\boldsymbol{e}_r\\ \boldsymbol{V}_{M/R_0}=\dot{r}\boldsymbol{e}_r+r\dot{\theta}\boldsymbol{e}_\theta+r\dot{\varphi}\sin\theta\boldsymbol{e}_\varphi\end{cases} \tag{3}$$

$\boldsymbol{V}_{M/R_0}$ thus obtained, is the sum of a relative speed $\boldsymbol{V}_r$ and a training speed $\boldsymbol{V}_e$ what are:

$$\begin{cases}\boldsymbol{V}_r=\dot{r}\boldsymbol{e}_r\\ \boldsymbol{V}_e=r\dot{\theta}\boldsymbol{e}_\theta+r\dot{\varphi}\sin\theta\boldsymbol{e}_\varphi\end{cases} \tag{4}$$

In this relationship $\dot{\varphi}$ represents the speed of rotation of the Earth and θ Co-latitude related to latitude λ by a relationship that we note:

$$\begin{cases}\dot{\varphi}=\omega_T=\dfrac{2\pi}{T}=\dfrac{2\pi}{24}\\ \theta=\dfrac{\pi}{2}-\lambda\rightarrow\sin\theta=\cos\lambda\end{cases} \tag{5}$$

If we consider a constant latitude λ given, θ will also be constant and therefore $\dot{\theta}=0$. So the speed is reduced to:

$$\boldsymbol{V}_{M/R_0}=\dot{r}\boldsymbol{e}_r+r\dot{\varphi}\cos\lambda\boldsymbol{e}_\varphi \tag{6}$$

Returning to our study context where $h(t)=r$ then the production speed $V_P(t)$ is deduced from the expression:

$$\begin{cases}\boldsymbol{V}_P(t)=\dot{h}\boldsymbol{e}_r+h\dot{\varphi}\cos\lambda\boldsymbol{e}_\varphi\\ V_P(t)=\sqrt{\dot{h}^2+\left(h\dot{\varphi}\cos\lambda\right)^2}\end{cases} \tag{7}$$

Finally, to show the variation in speed as a function of longitude φ containing

φ_0 we will express the spherical basis vectors as a function of the Cartesian basis vectors. We know that:

$$\begin{cases} \boldsymbol{e}_r = \sin\theta\cos\varphi\boldsymbol{i} + \sin\theta\sin\varphi\boldsymbol{j} + \cos\theta\boldsymbol{k} \\ \boldsymbol{e}_\varphi = -\sin\varphi\boldsymbol{i} + \cos\varphi\boldsymbol{j} \end{cases} \tag{8}$$

So we obtain the components V_{px}, V_{py}, V_{pz} of production speed with V_{pz} the component by which the vertical drift speed could be estimated.

$$\begin{cases} V_{px}(t) = \cos\lambda\left(\dot{h}\cos\varphi - h\dot{\varphi}\sin\varphi\right) \\ V_{py}(t) = \cos\lambda\left(\dot{h}\sin\varphi + h\dot{\varphi}\cos\varphi\right) \\ V_{pz}(t) = \dot{h}\sin\lambda \end{cases} \rightarrow \begin{cases} \dot{h}(t) = -\dfrac{\pi^2}{144}k\left[P_0(t) + 8\sin\left(\dfrac{\pi}{4}t\right)\right] \\ \varphi = \omega t - \varphi_0 \\ \omega = \dfrac{\pi}{12}; \varphi_0 \end{cases} \tag{9}$$

The production rate at a given geographical position is the result of the contribution of each of the three components as shown in the example at 6 o'clock in Figure 4 below at the Greenwich meridian of latitudes 0˚ and Longitude 0˚.

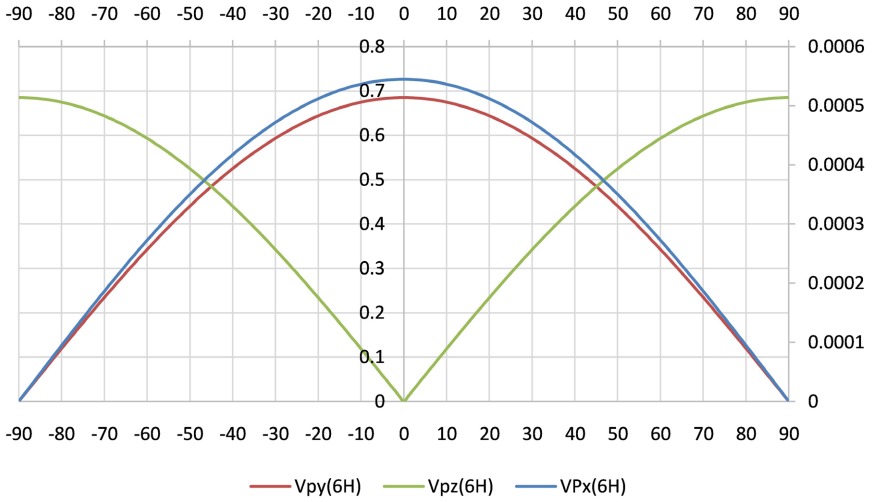

Figure 4. Profile of production speeds V_{px}, V_{py} and V_{pz} as a function of geographic latitudes $k = 1$.

The modulus of the V_{pz} component simulating the vertical drift increases from the equator to latitudes of 90˚ while those of the V_{px} and V_{py} components decrease. From then on, we understand that at a latitude λ and in the same longitude sector, the production following the vertical component will be almost symmetrical on either side of the two hemispheres and greater than that at the equator. The V_{pz} component, as evidenced by the global ionization volume (Figure 6 below), which also presents the same profile at these latitudes (0˚ to 37˚), is therefore the one that describes the equatorial ionization anomaly and not the resulting velocity, which decreases from the equator (Figure 5 below).

This therefore suggests that the share of solar radiation power received by each point is called power density $D_p(t)$ or solar irradiance $I(t)$ in W/m^2

would be increasing from the equator to the peaks of latitudes of ionization density maxima, justifying the equatorial ionization anomaly [12]. Which is true because even if the power of solar radiation in Watts by its amplitude "2k" is maximal at the equator, its distribution across the densification surface (given by the product of the coordinates $x(t)$ and $y(t)$) at the equator and near latitudes as shown in **Figure 6** is equally large but reduces considerably away from the equator.

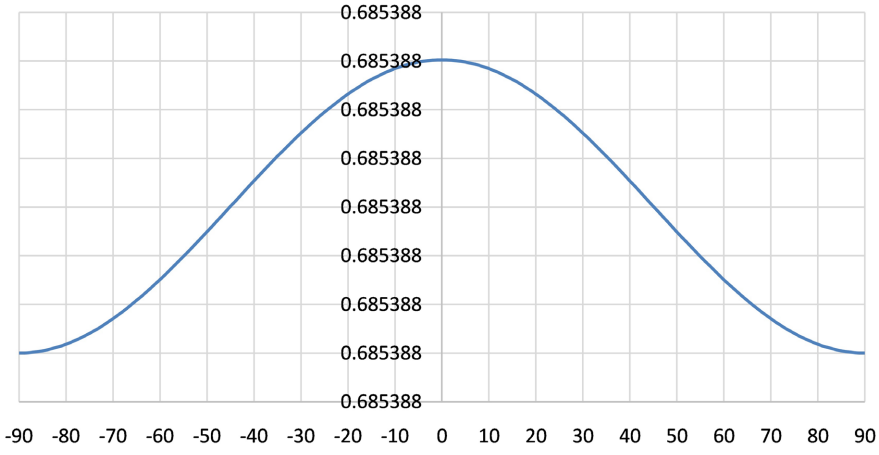

Figure 5. Profile of the resulting production rate of V_{px}, V_{py} and V_{pz} depending on the latitudes ($k = 1$).

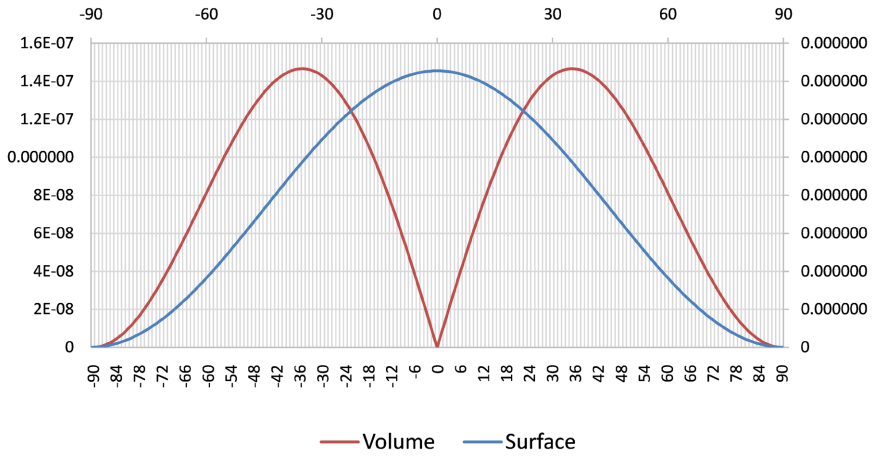

Figure 6. Latitudinal variation of the densification surface and the ionization volume with $k = 1$.

$$\begin{cases} x(t) = h\cos\lambda\cos\varphi \\ y(t) = h\cos\lambda\sin\varphi \\ z(t) = h\sin\lambda \end{cases} \rightarrow \begin{cases} S(t) = x(t)\cdot y(t); V(t) = S(t)\cdot z(t) \\ D_p(t) = \dfrac{k\cdot P_0(t)}{S(t)} \rightarrow w\cdot m^{-2} \\ D_p(t) = \dfrac{k\cdot P_0(t)}{V(t)} \rightarrow w\cdot m^{-3} \end{cases} \tag{11}$$

However, from a certain geographical latitude (37˚ - 38˚N and 37˚ - 38˚S) the

densification surface or the power of solar radiation in Watts has decreased by a certain proportion so that an increase in the power density will certainly produce ionization but not in sufficient volume or quantity compared to latitudes close to the equator, hence the decrease in ionization volume observed.

The fundamental physical statement that "the power of solar radiation is greater the further one moves away from the equator" is true for surface power density, *i.e.* in Watts per m^2, because this power density or irradiance is the quotient of the variation in the power of solar radiation on the surface of densification produced by the coordinates $x(t)$ and $y(t)$.

Finally the average diurnal production rates found are of the form:

$$V_{pz}(\lambda,k)_{moy} = 36.70\times10^{-2}k\sin\lambda \tag{10}$$

With 36.70×10^{-2} the average daytime speed of $\dot{h}$ from 0 h to 24 h. So for a speed $V_{pz}(\lambda,k)_{moy}$ constant the production factor "*K*" is decreasing as a function of latitudes (same profile as the module as the resulting speed) and for the same latitude the production factor is increasing linearly as a function of speeds.

3. Results

The temporal variability of the power of solar radiation being known, then the variable to be found or estimated is the coefficient of proportionality "*K*" and this in order to properly estimate the time profile of the vertical "drift" speed. To this end, let us consider as an example the profiles shown in Figure 7, obtained for latitudes of 5˚ and 10˚, where the velocity values are multiples of the factor *k*. For example on the graph the production speed 0.05 would actually represent 0.05 *k*.

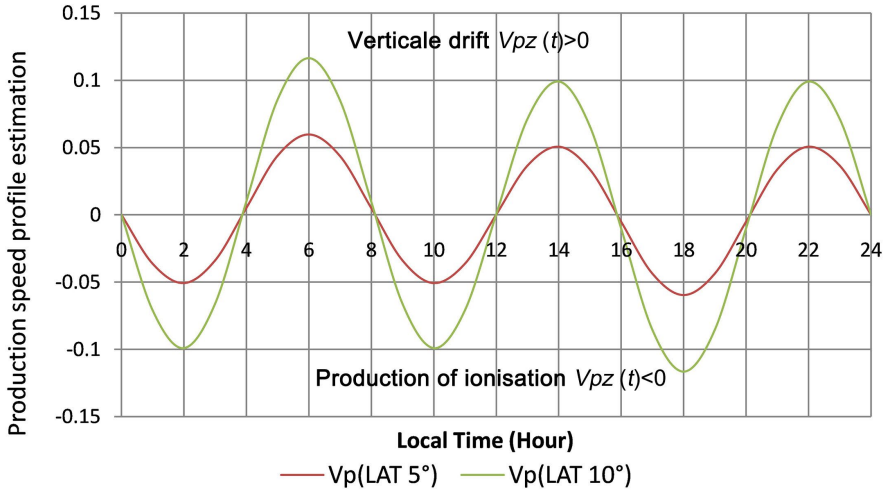

Figure 7. Velocity profiles of production for latitudes of 5˚ and 10˚ following *k*.

The obtained production speed profile shows that the movement of the HmF2 ionization densification surface is rectilinear and uniformly varied at all times of the day. Only the movement is: 1) Sometimes downwards for negative displacement speeds marking an increasingly pronounced production by photoionization.

Sometimes upwards marking an increasingly less pronounced production by photoionization for positive displacement speeds and this is due to the fact that the positive direction of the basic vector " $\boldsymbol{k}$ " of the Cartesian frame of reference is oriented upwards. We note that:

$$\boldsymbol{V}_{Pz}(t)=V_{pz}(t)\boldsymbol{k} \tag{12}$$

Thus a) For a positive production rate $V_{pz}(t)_1>0$ its maximum ionization density $NmF2\left(V_{pz}(t)_1\right)$ is lower than that $NmF2\left(V_{pz}(t)_2\right)$ of a negative production rate $V_{pz}(t)_2<0$ most often for very close times due to the decrease in the power of the solar radiation. We will then note that:

$$\begin{cases} V_{pz}(t)_1>0 \text{ and } V_{pz}(t)_2<0 \\ NmF2\left(V_{pz}(t)_2\right)>NmF2\left(V_{pz}(t)_1\right) \end{cases} \tag{13}$$

b) Also if:

$$\begin{cases} V_{pz}(t)_1>0; V_{pz}(t)_2>0 \\ \text{and } V_{pz}(t)_1>V_{pz}(t)_2 \\ NmF2\left(V_{pz}(t)_1\right)<NmF2\left(V_{pz}(t)_2\right) \end{cases} \tag{14}$$

c) Finally if:

$$\begin{cases} V_{pz}(t)_1<0; V_{pz}(t)_2<0 \\ \text{and } \left|V_{pz}(t)_1\right|>\left|V_{pz}(t)_2\right| \\ NmF2\left(V_{pz}(t)_1\right)>NmF2\left(V_{pz}(t)_2\right) \end{cases} \tag{15}$$

2) Thus described the plasma appears initially in the state (P_0,V_0). a) A negative production rate will make it pass to the state (P_1,V_1) even denser because the pressure P_1 is higher than that of P_0 and the volume V_1 lower than that of V_0

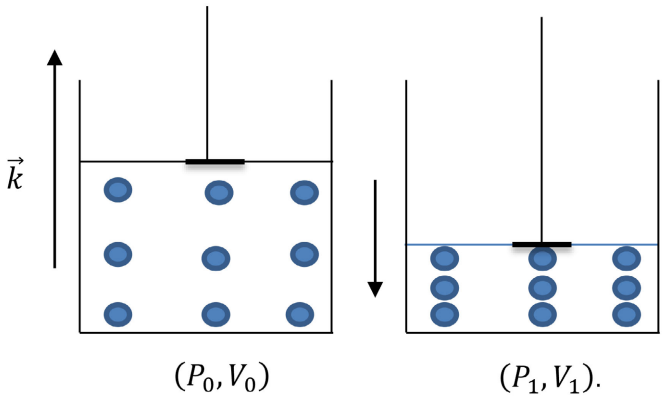

b) A positive production rate will make it pass to the state (P_2,V_2) even less dense because the pressure P_2 is lower than that of P_0 and the volume V_2 higher than that of V_0

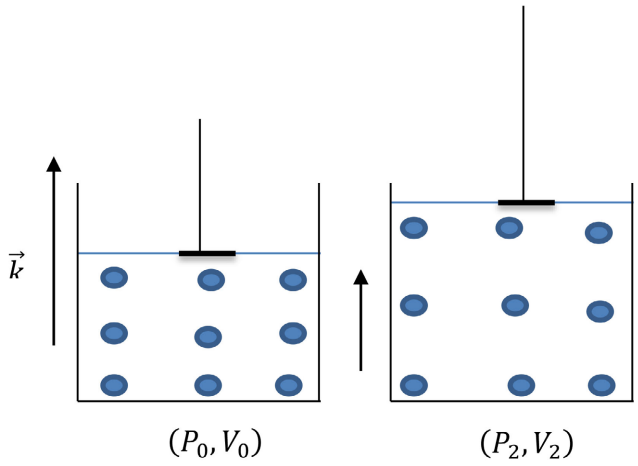

3) Positive speeds reflect less densification, so positive production speeds are those that describe vertical drift. 4) However, vertical drift speeds do not reflect an absence of production but rather production speeds inversely proportional to the vertical drift speed.

$$\begin{cases} \text{if } V_d(t) \neq 0 \rightarrow V_{pz}(t) = \dfrac{C_0}{V_d(t)} \\ \text{if } V_d(t) = 0 \rightarrow V_{pz}(t) = 0 \end{cases} \tag{16}$$

Thus the graph in Figure 7 above shows us: 1) During the day, a production trough centered around 2 p.m. is separated by two production peaks which are much more steep for latitudes further and further from the equator than those closer and closer. The production trough marks a drop in production speed by photoionization, thus justifying the vertical drift. The two production peaks, one in the morning around 10 a.m. and the other in the afternoon around 6 p.m., justifying the interpretation of an electrojet in the morning and a counter-electrojet in the evening, which are, however, inflection points marking production peaks due to the effect of the Earth's rotation. This vertical drift centered around 2 p.m. is also more pronounced at latitudes further away than those closer to the equator. 2) At night, corspuscular ionization by energetic particles and recombination mechanisms supplement photoionization. Corspuscular ionization becomes predominant from 6 p.m. to 10 p.m. and from 2 a.m. to 6 a.m. in the high altitude layers and recombinations in the lower layers. From 10 p.m. to 2 a.m., recombinations now become predominant in the high layers and corspuscular ionization in the lower layers, thus allowing a night peak to be obtained in this time range. Finally, through the variability in modulus or intensity of drift and production velocities as shown in Figure 8 below, an estimate of the profile of the variability of foF2 frequencies can be established, further materializing the vertical drift.

Of the different peaks, those of 6 H and 18 H have the highest velocity amplitudes preceded by the other peaks which have the same amplitudes. However, as the peak of 6 H is a drift, its ionization density and consequently its critical frequency foF2 will be the lowest, unlike that of 18 H which corresponds to a pro-

duction which will have the highest critical frequency. Of the other drift peaks 14 H and 22 H, that of 14 H will have a more raised amplitude of foF2 than that of 22 H because this drift occurred during the day. However, the peak of 14 H will be less raised in foF2 than that of 10 H because it is a production but more raised than the production peak of 2 H taking place during the night. The peak of 2 H will be more raised than that of 22 H because it is a production. Finally, of two drift peaks occurring at the same time, the one with the lowest amplitude will have the highest critical frequency foF2. On the other hand, of two production peaks occurring at the same time, the one with the highest speed will also have the highest critical frequency foF2. From these different peaks or observation points, an estimate of the profiles can be established, as shown in the Figure 9 below. However, with regard to ionospheric dynamics, we will speak more of a propensity to observe peaks at such a time. Thus, we will have a greater propensity to observe the 6 a.m. peak between 5 a.m. and 7 a.m., the 10 a.m. peak between 9 a.m. and 11 a.m., the 2 p.m. peak between 1 p.m. and 3 p.m., the 6 p.m. peak between 5 p.m. and 7 p.m., the 10 p.m. peak between 9 p.m. and 11 p.m., and finally the 2 a.m. peak between 1 a.m. and 3 a.m.

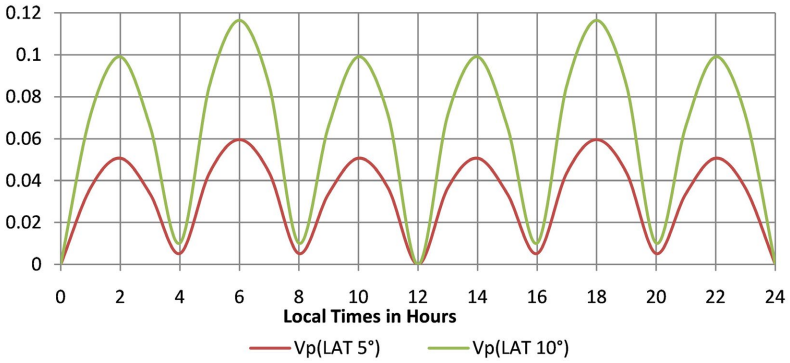

Figure 8. Temporal variability in modulus of drift and production speeds.

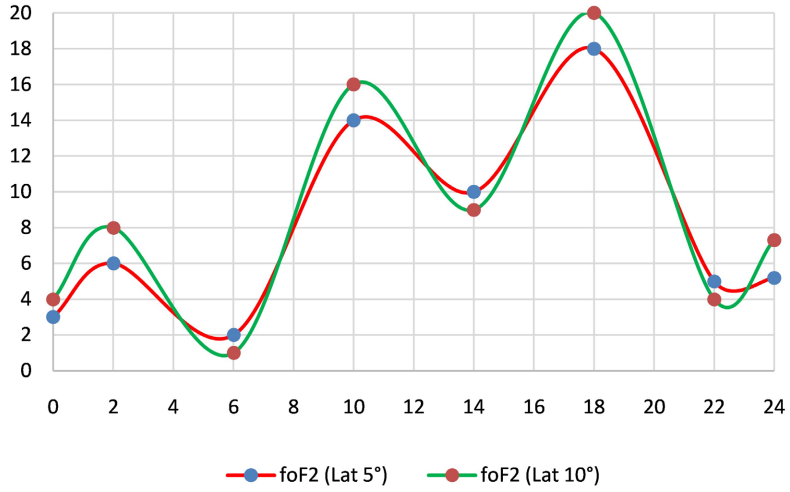

Figure 9. Estimation of diurnal profiles of foF2 variability (MHz) showing drifts and productions.

4. Discussion

4.1. Estimation of Production Factor and Average Speed by Radar Data: Jicamarca Radar

From radar data for example from Jicamarca (the precursor) located at latitude 10˚S and taking as reference the evening peak due to its very large fluctuation as shown in Figure 10 below modeled by [9] we can give an estimate of the speed factor as well as the average production speed.

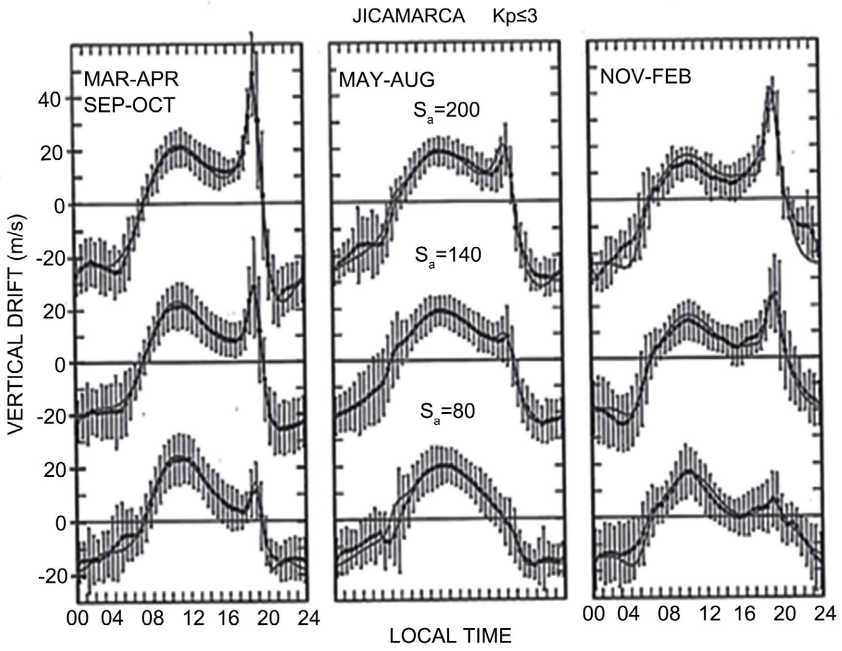

Figure 10. Scherliess and Fejer model of vertical drift using Jicamarca radar data.

For example: 1) For Latitudes of 3˚ as shown in Figure 11 below and a) for an evening peak at 40 $m{\cdot}s^{-1}$ the production factor found in the models is approximately 1320 and the estimated average diurnal speed is 25.20 $m{\cdot}s^{-1}$ (0 H to 24 H). b) On the other hand, for an evening peak at 60 $m{\cdot}s^{-1}$ the factor is at 1980 and the estimated average speed is 37.79 $m{\cdot}s^{-1}$.

c) Thus the vertical drift in the afternoon from 12 H to 16 H centered at 14 H at latitude of 3˚ as shown in Figure 11 below has a speed peak at 14 H of 60 $m{\cdot}s^{-1}$ and of 40 $m{\cdot}s^{-1}$ respectively for production factors $k \cong 1980$ and 1320. (d) On the other hand, for the morning vertical drift from 4 a.m. to 8 a.m. at latitude 3˚ as shown in Figure 11 below, we would observe a peak drift speed at 6 a.m. 71 $m{\cdot}s^{-1}$ and of 47 $m{\cdot}s^{-1}$ respectively for production factors $k \cong 1980$ and 1320.

Not losing sight of the fact that the production speed is inversely proportional to the drift speed, then the production will be increasingly increasing from the vertical drift peaks to the production peaks (6 a.m. to 10 a.m. and 2 p.m. to 6 p.m. and from 10 p.m. to 2 a.m.) and will be increasingly decreasing from the production peaks to the vertical drift peaks (2 a.m. to 6 a.m., 10 a.m. to 2 p.m. and from 6 p.m. to 10 p.m.).

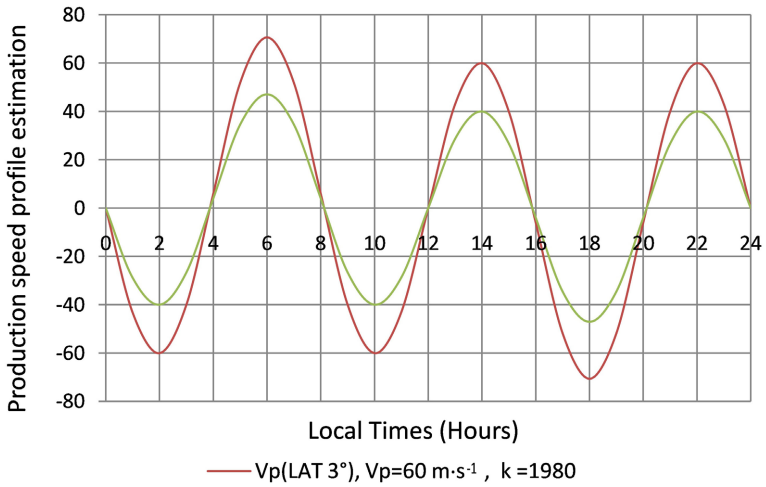

Figure 11. Modeling of production at latitudes 3˚.

2) For latitudes of 5˚ we obtain the same ionization profiles with the same production and drift rates. Only the production factor changes. Thus: a) For an evening peak at 40 $m \cdot s^{-1}$ the factor is now at 790 and the estimated average speed is 25.21 $m \cdot s^{-1}$; b) For an evening peak at 60 $m \cdot s^{-1}$ the factor is now at 1185 and the estimated average production speed 37.83 $m \cdot s^{-1}$.

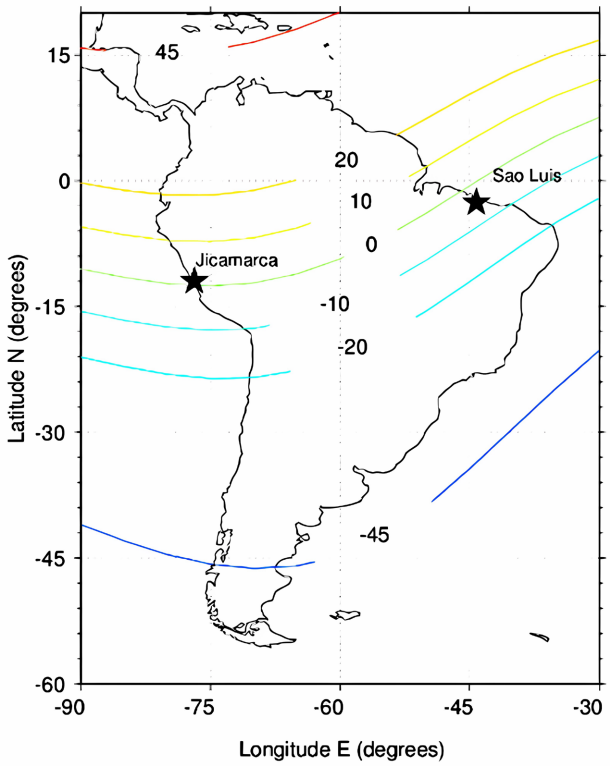

https://www.researchgate.net/publication/337141182/figure/fig1/AS:11431281250548529@1717926787980/Map-of-South-America-showing-the-location-of-the-Sao-Luis-site-where-the-MELISSA-radar.png (Source).

Figure 12. Jicamarca is located at geographic latitude 10˚ and magnetic equator 0˚.

Finally, if we consider the city of Jicamarca itself located at the geographical latitude of 10˚S as shown in Figure 12 above, we will see that the production factor will be lower:

a) And for an evening peak at 40 $m \cdot s^{-1}$ the factor is 397 and the estimated average speed is 25.19 $m \cdot s^{-1}$.

b) For an evening peak at 60 $m \cdot s^{-1}$ the factor is at 596 and the estimated average production speed is 37.83 $m \cdot s^{-1}$.

4.2. Estimation of Production Factor and Average Speed with IRI 2020

If the proposed model has made it possible to find the temporal profile of ionization by adjusting the production factor using radar data, what will happen with the data from the IRI-2020 model? Indeed, IRI is an international reference model for ionospheric issues. Several versions have been developed and used in modeling as an approximate model of the reality given by the results of in situ measurements. IRI can therefore provide the estimated profile of the vertical drift for any geographical position. However, for the present case, the cities of Conakry and Sikasso are dedicated to it, taking into account recent work published [13] on the vertical drift of ionization of these two cities using the differential method developed by [14]. The dates of the quiet days are 19/02/1993 (AIEE International Year of Equatorial Electrojet magnetic field measurement campaign) [15] for Sikasso and 20/08/2008 (AMBER African Magnetic B-field Education and Research magnetic field measurement campaign) for Conakry. These two cities are located at the following geographical positions in Table 1 below:

Table 1. Geographic position.

Name of station	Geo.Lat	Geo.Long
Conakry	10.5˚N	5.706˚W
Sikasso	11.344˚N	13.71˚W

After validation with IRI 2020 we obtain the following graphs giving the vertical drift profiles in $m \cdot s^{-1}$ respectively for Conakry (Figure 13) and Sikasso (Figure 14).

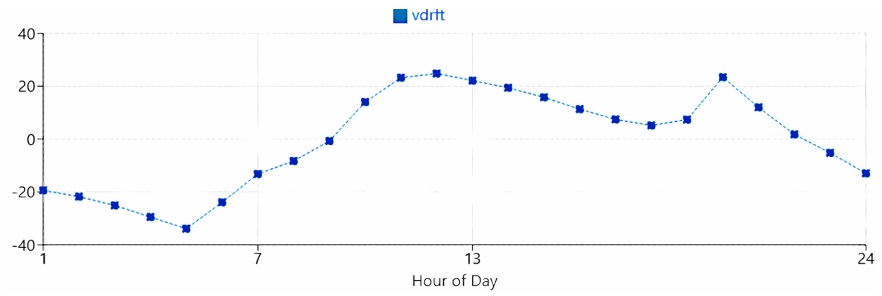

Figure 13. Profile of the vertical drift IRI-2020 Conakry on 08/20/2013 on a day of magnetic calm.

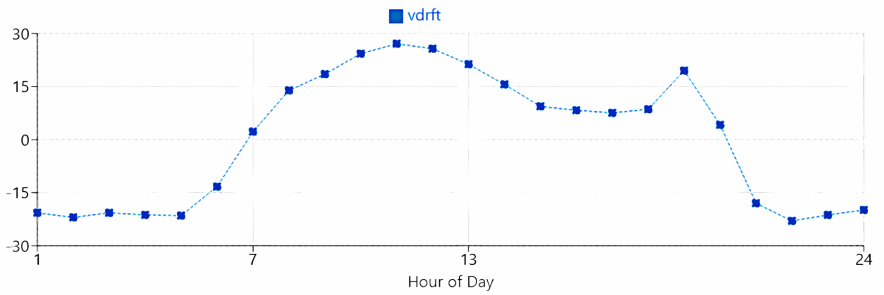

Figure 14. Profile of the vertical drift IRI-2020 Sikasso on 02/19/1993 on a day of magnetic calm.

These types of profiles show that during the magnetic calm day, the drift will have a dome structure with a peak centered at local noon (12:00). This contrasts somewhat with the proposed model because the ionization a priori presents two production peaks, one in the morning and the other in the afternoon, a little more prominent, and two drift peaks also in the early morning and in the afternoon. The dome profile can only appear during periods or time slots of vertical drift.

Thus, for this modeling purpose, using the proposed model, knowing the average vertical drift speed from the IRI 2020 data, the production factors for each city can be calculated. Once this is done, we could go back and find the profile of both the vertical drift and the production. The production factor is given as a reminder by the formula:

$$\begin{cases} V_p(\lambda,k)_{moy} = 36.70\times10^{-2} k \sin\lambda \\ k = \dfrac{V_p(\lambda,k)_{moy}}{36.70\times10^{-2}\sin\lambda} \end{cases}$$

$V_p(\lambda,k)_{moy}$ being the average daily speed from 0 H to 24 H obtained by transforming all negative values into positive values. Negative speeds only indicate the return or opposite movement to the direction taken as positive of the chosen reference frame. Thus:

a) The average speed found for the city of Conakry is 15.90 $m{\cdot}s^{-1}$ the calculated production factor of 240.69.

b) The average speed found for the city of Sikasso is 16.99 $m{\cdot}s^{-1}$ the calculated production factor of 236.19.

Thus the morning drift of the two cities is presented in the following form **Figure 15** below indicating the maximum speeds of the morning drift centered at 6 a.m. respectively of 30.02 $m{\cdot}s^{-1}$ for the city of Conakry and 31.89 $m{\cdot}s^{-1}$ for that of Sikasso.

The afternoon vertical drift presents the following profile in **Figure 16** below indicating the maximum speeds of the drift in the afternoon centered at 2 p.m. respectively 25.52 $m{\cdot}s^{-1}$ for the city Conakry and of 27.11 $m{\cdot}s^{-1}$ for that of Sikasso.

Finally, there are other methods for estimating the speed of drifts such as the rate of variation of the maximum ionization density height HmF2 [16] and [17]

or the virtual height h'F2 [18] and [19] or simply with ionosonde data [20] and [21] and also the differential method which is based on magnetometer data.

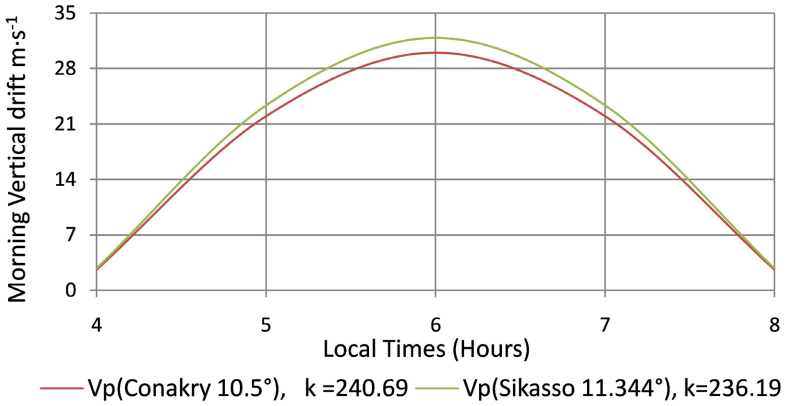

Figure 15. Morning drift for the cities of Conakry and Sikasso.

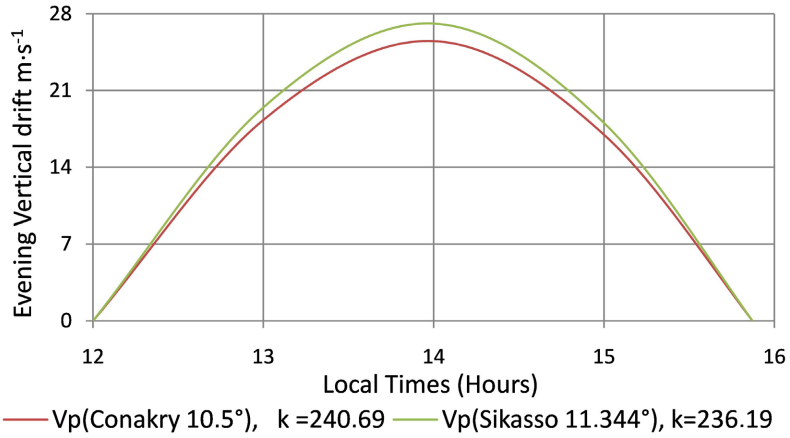

Figure 16. Afternoon drift for the cities of Conakry and Sikasso.

4.3. Importance

The model proposed by the ionization production speed simulates reality very well. By this model are highlighted: 1) The day the trough as well as the two peaks of production. 2) The night peaks. 3) The fluctuations of the height of maximum ionization HmF2 as well as the density of the maximum ionization NmF2. 4) By this model and through the different peaks one can also estimate the profile of the variability of the critical frequencies foF2. Thus for days of magnetic calm by referring to radar data from Jicamarca or any other by the peak speed at the beginning of the night one can find the profile of ionization production, vertical drift, the production factor as well as the average diurnal speed from 0 H to 24 H and day from 4 H to 20 H at each latitude. Also, with IRI 2020 knowing the average speed of the vertical drift, we can find the production factor of any location and then go back to find the profile of both the drift and the production. Also, the proposed method indicates the time ranges of vertical drift and those of production. Finally, using the production factor, we can also proceed to modeling ac-

cording to seasons, phases of the solar cycle, etc. As a perspective, we propose to analyze ionization according to longitudes.

5. Conclusion

At the end of this article, it is clear that the production rate is proportional to the variability of the power of solar radiation. This coefficient of proportionality will be called the power or production factor and for the same ionization, it is lower and lower the further one moves away from the equator. This thus shows that the power density of solar radiation is greater the further one moves away from the equator and that a small variability in this power density of this solar radiation will have the same effect, if not more than a large temporal variability at latitudes even closer to the equator. The production rate results from the contribution of the three components and the one capable of showing or simulating the vertical drift is the Vpz component. The modeling of the production rate by referring to the incoherent scattering radar data from Jicamarca and by IRI 2020 was quite satisfactory. By this modeling we show that by the proposed model, we can find the ionization profile, the factor as well as the average production rate at each latitude.

Conflicts of Interest

The authors declare no conflicts of interest regarding the publication of this paper.

References

[1] Anderson, D.N. (1973) A Theoretical Study of the Ionospheric F Region Equatorial Anomaly—II. Results in the American and Asian Sectors. *Planetary and Space Science*, **21**, 421-442. https://doi.org/10.1016/0032-0633(73)90041-x

[2] Appleton, E.V. (1946) Two Anomalies in the Ionosphere. *Nature*, **157**, 691-691. https://doi.org/10.1038/157691a0

[3] Bramley, E.N. and Peart, M. (1965) Diffusion and Electromagnetic Drift in the Equatorial *F*2-Region. *Journal of Atmospheric and Terrestrial Physics*, **27**, 1201-1211. https://doi.org/10.1016/0021-9169(65)90081-4

[4] Reddy, C.A. (1989) The Equatorial Electrojet. In: Campbell, W.H., Ed., *Quiet Daily Geomagnetic Fields*, Birkhäuser Basel, 485-508. https://doi.org/10.1007/978-3-0348-9280-3_11

[5] Gouin, P. and Mayaud, P.N. (1967) A propos de l'existence possible d'un contre electrojet aux latitudes magnétiques équatoriales. *Annales Geophysicae*, **23**, 41-47.

[6] Abdu, M.A. (1997) Major Phenomena of the Equatorial Ionosphere-Thermosphere System under Disturbed Conditions. *Journal of Atmospheric and Solar-Terrestrial Physics*, **59**, 1505-1519. https://doi.org/10.1016/s1364-6826(96)00152-6

[7] Coley, W.R., Stoneback, R.A., Heelis, R.A. and Hairston, M.R. (2014) Topside Equatorial Zonal Ion Velocities Measured by C/NOFS during Rising Solar Activity. *Annales Geophysicae*, **32**, 69-75. https://doi.org/10.5194/angeo-32-69-2014

[8] Woodman, R.F. (1970) Vertical Drift Velocities and East-West Electric Fields at the Magnetic Equator. *Journal of Geophysical Research*, **75**, 6249-6259. https://doi.org/10.1029/ja075i031p06249

[9] Scherliess, L. and Fejer, B.G. (1999) Radar and Satellite Global Equatorial *F* Region Vertical Drift Model. *Journal of Geophysical Research*: *Space Physics*, **104**, 6829-6842. https://doi.org/10.1029/1999ja900025

[10] Alken, P. (2009) A Quiet Time Empirical Model of Equatorial Vertical Plasma Drift in the Peruvian Sector Based on 150 Km Echoes. *Journal of Geophysical Research*: *Space Physics*, **114**, AO2308. https://doi.org/10.1029/2008ja013751

[11] Abdoul-kader, S., Allain, G.D. and Aristide, G. (2023) New Analysis of the Seasonal Variation of the Critical Frequencies Fof2 by a Proposed Formula of the Power of Solar Radiation. *International Journal of Geophysics*, **2023**, Article ID 4405266. https://doi.org/10.1155/2023/4405266

[12] Segda, A.K., Kaboré, S., Gybre, A. and Ouattara, F. (2025) Equatorial Ionization Anomaly (EIA) under the Solar Radiation Spectrum. *Journal of Modern Physics*, **16**, 754-773. https://doi.org/10.4236/jmp.2025.165041

[13] Kassamba, A.A., Doumbia, V., Obrou, O.K., Grodji, F.O., Tuo, Z., Kouassi, N., *et al.* (2020) Estimating the Daytime Vertical E × B Drift Velocities in the F-Region of the Equatorial Ionosphere Using the IEEY and AMBER Magnetic Data in West Africa. *Advances in Space Research*, **65**, 2573-2585. https://doi.org/10.1016/j.asr.2020.03.008

[14] Anderson, D., Anghel, A., Chau, J. and Veliz, O. (2004) Daytime Vertical E × B Drift Velocities Inferred from Ground-Based Magnetometer Observations at Low Latitudes. *Space Weather*, **2**, S11001. https://doi.org/10.1029/2004sw000095

[15] Amory-Mazaudier, C. (2018) International Equatorial Electrojet Year: The African Sector. *Brazilian Journal of Geophysics*, **11**, 303-317. https://doi.org/10.22564/rbgf.v11i3.1152

[16] Obrou, O.K., Bilitza, D., Adeniyi, J.O. and Radicella, S.M. (2003) Equatorial F2-Layer Peak Height and Correlation with Vertical Ion Drift and M(3000)F2. *Advances in Space Research*, **31**, 513-520. https://doi.org/10.1016/s0273-1177(03)00024-3

[17] Adebesin, B.O., Adeniyi, J.O., Adimula, I.A. and Reinisch, B.W. (2013) Equatorial Vertical Plasma Drift Velocities and Electron Densities Inferred from Ground-Based Ionosonde Measurements during Low Solar Activity. *Journal of Atmospheric and Solar- Terrestrial Physics*, **97**, 58-64. https://doi.org/10.1016/j.jastp.2013.02.010

[18] Lee, C.-C., Liu, J.-Y., Reinisch, B.W., Chen, W.-S. and Chu, F.-D. (2005) The Effects of the Pre-Reversal E × B Drift, the EIA Asymmetry, and Magnetic Activity on the Equatorial Spread F during Solar Maximum. *Annales Geophysicae*, **23**, 745-751. https://doi.org/10.5194/angeo-23-745-2005

[19] Uemoto, J., Maruyama, T., Saito, S., Ishii, M. and Yoshimura, R. (2010) Relationships between Pre-Sunset Electrojet Strength, Pre-Reversal Enhancement and Equatorial Spread-F Onset. *Annales Geophysicae*, **28**, 449-454. https://doi.org/10.5194/angeo-28-449-2010

[20] Oyekola, O.S. and Kolawole, L.B. (2010) Equatorial Vertical E × B Drift Velocities Inferred from Ionosonde Measurements over Ouagadougou and the IRI-2007 Vertical Ion Drift Model. *Advances in Space Research*, **46**, 604-612. https://doi.org/10.1016/j.asr.2010.04.003

[21] Grodji, F.O., Doumbia, V., Boka, K., Amory-Mazaudier, C., Cohen, Y. and Fleury, R. (2017) Estimating Some Parameters of the Equatorial Ionosphere Electrodynamics from Ionosonde Data in West Africa. *Advances in Space Research*, **59**, 311-325. https://doi.org/10.1016/j.asr.2016.09.004